Mecánica Computacional Vol. XXIV
A. Larreteguy (Editor)
Buenos Aires, Argentina, Noviembre 2005

A NUMERICAL TECHNIQUE FOR SIMULATING VISCOELASTIC FREE SURFACE FLOWS USING THE K-BKZ INTEGRAL CONSTITUTIVE EQUATION

Manoel S. B. Araujo [*], **Murilo F. Tomé** [*], **José A. Cuminato** [*], **A. Castelo** [*], **V. G. Ferreira** [*]

[*]Departamento de Matemática Aplicada e Estatística, ICMC - USP São Carlos,
Universidade de São Paulo,
Av. Trabalhador Saocarlense, 400, C.P. 668, 13251-900, São Carlos, Brasil
e-mail: murilo@icmc.usp.br

Key Words: K-BKZ constitutive equation, viscoelastic flow, finite difference, free surface.

Abstract. *This work presents a numerical technique for simulating viscoelastic free surface flows governed by the K-BKZ integral constitutive equation. The numerical method solves the governing equations using the finite difference method on a staggered grid. The equation of motion is integrated by the GENSMAC methodology. The fluid surface is modeled by the marker-and-cell method which provides the visualization and the location of the fluid free surface. The full free surface stress conditions are employed. The Finger tensor is computed using the ideas of the deformation fields method. The integrand of the integral constitutive equation is approximated by a linear piecewise function which is integrated exactly and the transport term of the Finger strain tensor is approximated by a high order upwind scheme. Numerical results showing the convergence of the numerical method developed in this work for the flow in a two-dimensional channel are presented. In addition, the simulations of the flow through a planar 4:1 contraction and jet buckling are given.*

1 Introduction

The majority of numerical techniques for simulating viscoelastic fluid flows employs differential constitutive models. An advantage of this approach is that the evolution of the stress depends on the velocity and stress fields only. Over the past 20 years differential models have been numerically studied by many researchers using finite element,[1–4] finite volume[5,6] and finite difference methods.[7] Nonetheless, numerical methods for solving integral viscoelastic models have also been employed most of them using the finite element method.[8–11] In particular, the KBKZ integral model has been considered a realistic constitutive model for solving industrial polymer flows.[9,12,13]

The main objective of this work is to present a finite difference technique for simulating flows governed by the integral K-BKZ constitutive equation. The conservation equations are solved following the approach used by Tomé et al.[7] To calculate the stress tensor we employ the ideas of the deformation fields method introduced by Peters et al.[9] This approach allows the Finger tensor to be calculated without the necessity of following a fluid particle. In their paper, Peters et al.[9] use the fact that the upper-convected derivative of the Finger tensor is null in order to convect the Finger tensor in time. More recently, Hulsen et al.[14] pointed out the fact that this approach had some drawbacks and proposed a modification by adding a term containing a derivative in respect to the elapsed time $s = t - t'$ into the upper-convected derivative. However, by using finite differences this modification is not necessary if the weights used to calculate the stress tensor are not constants; they depend on the present time t. Therefore the integral of the constitutive equation is calculated by using the past time t', not the elapsed time s. This procedure implies to recalculate the values of t' used at each time t.

This paper is organized as follows. Section 2 presents the basic equations together with the boundary conditions; section 3 gives the discretisation of the reference time and the approximation of the extra-stress tensor. In sections 5 and 6 the GENSMAC algorithm and the main finite difference equations are given. Finally, in section 7 we present the numerical results obtained for the flow in a two-dimensional channel and for the flow through a planar 4:1 contraction and jet buckling of a fluid modeled by the K-BKZ constitutive equation.

2 Governing equations

The basic equations governing isothermal incompressible flows are the continuity equation

$$\nabla \cdot \mathbf{v} = 0 \,, \tag{1}$$

and the momentum equation

$$\rho_0 \left[\frac{\partial \mathbf{v}}{\partial t} + \nabla \cdot (\mathbf{v}\,\mathbf{v}) \right] = -\nabla p + \nabla \cdot \boldsymbol{\tau} + \rho_0 \mathbf{g} \,, \tag{2}$$

where $\frac{D}{Dt}$ is the material derivative, ρ_0 is the density, $\mathbf{v}$ is the velocity vector, p is the pressure, $\mathbf{g}$ is the gravity and $\boldsymbol{\tau}$ is the extra-stress tensor. In this work the extra-stress tensor is given by the K-BKZ constitutive equation

$$\boldsymbol{\tau}(t) = \int_{-\infty}^{t} M(t-t') H(I_1, I_2) \mathbf{B}_{t'}(t)\, dt' \tag{3}$$

where $M(t-t')$ is the memory function, $H(I_1, I_2)$ is the dumping function and $\mathbf{B}_{t'}(t)$ is the Finger tensor measuring the deformation of a fluid particle at current time t with respect to the reference time t'.

I_1 and I_2 are the first and second invariant of $\mathbf{B}_{t'}(t)$ respectively. We will use the Papanastasiou, Scriven and Macosko (PSM) model[15] where

$$M(t-t') = \sum_m \frac{a_m}{\lambda_m} e^{-\frac{t-t'}{\lambda_m}} \tag{4}$$

and

$$H(I_1, I_2) = \frac{\alpha}{\alpha + \beta I_1 + (1-\beta) I_2} \,. \tag{5}$$

The constants a_m, λ_m, α and β are given material parameters. For simplicity we use only one relaxation parameter a_1 and λ_1. The procedure using more constants is similar. Details on the calculation of the Finger tensor will be given in the next section.

In order to solve equations (1)-(3) we employ the splitting

$$\boldsymbol{\tau} = \mathbf{S} + \eta_0 \dot{\boldsymbol{\gamma}} \tag{6}$$

where $\dot{\boldsymbol{\gamma}} = \nabla \mathbf{v} + (\nabla \mathbf{v})^{\mathrm{T}}$ is the rate-of-strain tensor and η_0 is the viscosity at low shear rates and $\mathbf{S}$ is a non-Newtonian tensor responsible for the viscoelastic effects in the flow. Introducing (6) into the momentum equation (2) it can be written as

$$\rho_0 \left[\frac{\partial \mathbf{v}}{\partial t} + \nabla \cdot (\mathbf{v}\,\mathbf{v}) \right] = -\nabla p + \eta_0 \nabla^2 \mathbf{v} + \nabla \cdot \mathbf{S} + \rho_0 \mathbf{g} \,. \tag{7}$$

Let $L, U, g, \eta_0, \rho_0, \lambda_1$ be characteristics values of length, velocity, gravity, viscosity, density and relaxation time, respectively. The nondimensional form of equations (1), (7), (3) and (6) can be obtained by using the nondimensional variables:

$$\bar{\mathbf{v}} = \frac{\mathbf{v}}{U},\ \bar{\mathbf{x}} = \frac{\mathbf{x}}{L},\ \bar{t} = \frac{U}{L} t,\ \bar{\mathbf{g}} = \frac{\mathbf{g}}{g},\ \bar{p} = \frac{p}{\rho_0 U^2},\ \bar{\mathbf{S}} = \frac{\mathbf{S}}{\rho_0 U^2},\ \bar{\eta} = \frac{\eta}{\eta 0},\ \bar{\rho} = \frac{\rho}{\rho 0},\ \bar{\lambda} = \frac{\lambda}{\lambda_1},\ \bar{a}_1 = \frac{a_1}{\rho_0 U^2} \,.$$

After introducing these nondimensional variables into equations (1), (7), (3) and (6) and omitting the bars we obtain the following non-dimensional equations

$$\nabla \cdot \mathbf{v} = 0 \,, \tag{8}$$

$$\frac{\partial \mathbf{v}}{\partial t} + \nabla \cdot (\mathbf{v}\,\mathbf{v}) = -\nabla p + \frac{1}{Re} \nabla^2 \mathbf{v} + \nabla \cdot \mathbf{S} + \frac{1}{Fr^2} \mathbf{g} \,, \tag{9}$$

$$\boldsymbol{\tau}(t) = \int_{-\infty}^{t} \frac{a_1}{We} e^{-\frac{t-t'}{We}} \frac{\alpha}{\alpha - 3 + \beta I_1 + (1-\beta) I_2} \mathbf{B}_{t'}(t) dt' \,, \tag{10}$$

$$\mathbf{S} = \boldsymbol{\tau} - \frac{1}{Re} \dot{\boldsymbol{\gamma}} \,, \tag{11}$$

where $Re = \frac{\rho_0 U L}{\eta_0}$ is the Reynolds number and $We = \lambda_1 \frac{U}{L}$ is the Weissenberg number. In this work we shall consider Cartesian two-dimensional flows with $\mathbf{v} = (u, v)$ and $\mathbf{x} = (x, y)$.

Therefore, in order to simulate two-dimensional flows governed by the K-BKZ constitutive equation we have to solve equations (8)-(11) subject to initial and boundary conditions.

Boundary conditions

For the momentum equations we impose the no-slip condition on rigid boundaries and on inflows the velocity is prescribed by a parabolic Newtonian profile. On outflows we take $\frac{\partial v_n}{\partial n} = 0$ and $\frac{\partial v_m}{\partial n} = 0$, where n and m denote normal and tangential directions to the outflow, respectively.

Free surface stress conditions

We consider transient free surface flows of viscous fluid flowing into a passive atmosphere and neglect surface tension effects. In this case, the appropriate boundary conditions on the free surface can be written as (see Tomé et al.[7])

$$\mathbf{n} \cdot (\boldsymbol{\sigma} \cdot \mathbf{n}) = 0 \qquad \text{and} \qquad \mathbf{m} \cdot (\boldsymbol{\sigma} \cdot \mathbf{n}) = 0 \tag{12}$$

where **n** and **m** denote unit normal and tangent vectors to the surface $\boldsymbol{\sigma}$ is the stress tensor given by

$$\boldsymbol{\sigma} = -p\mathbf{I} + \boldsymbol{\tau}$$

and $\boldsymbol{\tau}$ is the extra-stress tensor given by (6). The finite difference equations approximating these conditions will be given in Section 6.

3 Calculation of the extra-stress tensor

To compute the extra-stress tensor it is first necessary to discretize the interval $[0,\ t]$ to define the integration points t'_i. The maximum value of t', t'_{max}, is the time t ($t'_{max} = t$) and the interval $[0, t'_{max}]$ is then divided into N subintervals $[t'_{i-1}, t'_i]\ \ , i = 1, ..., N$, For a fixed time t the memory function is a fast decaying function for small values of t' and it is not necessary to take equal values for the size of $\Delta t'_i = t'_i - t'_{i-1}$. Thus, the size of $\Delta t'_i$ for t'_i near t has to be smaller than the size of $\Delta t'_i$ for t'_i near zero. We can split the interval in a number of different ways. In this work we use a more simple and direct discretization of t'. The interval $[M(0), M(t'_{max})]$ is divided into N equally spaced subintervals $[M(t'_{i-1}),\ (M(t'_i)]$ for $i = 1, 2, \cdots N$. The values of t'_i are the inverse image of the points $M(t'_i)$ and are given by

$$t'_i = We\, \ln\left[\frac{We}{a_1}\, M(t'_i)\right] + t\ . \tag{13}$$

Figure 1(a) shows the discretization of the interval $[M(0),\ M(t'_{max})]$. To avoid that points accumulate near t'_{max} for large values of t, we impose some condition on the size of $\Delta t'_i$. For instance, let $K > 0$ be given. if $\Delta t'_i > \frac{t}{K}$ we take $t'_i = t'_{i-1} + \frac{t}{K}$ and the interval $[M(t'_i), M(t'_{max})]$ is divided again into the remaining number of intervals. In the results shown in this paper we used $K = 15$. Having obtained the integration points $t'_i, i = 1, 2, \cdots, N$, the computation of the the extra-stress is performed as follows.

First we write the constitutive equation (10) as

$$\boldsymbol{\tau}(t) = \int_{-\infty}^{0} \frac{a_1}{We} e^{\frac{t'}{We}} F(\mathbf{B}_{t'}(0))dt' + \int_{0}^{t} \frac{a_1}{We} e^{-\frac{(t-t')}{We}} F(\mathbf{B}_{t'}(t))dt' \tag{14}$$

where the function $F(\mathbf{B}_{t'}(t))$ is given by

$$F(\mathbf{B}_{t'}(t)) = \frac{\alpha \mathbf{B}_{t'}(t)}{\alpha - 3 + \beta I_1 + (1-\beta) I_2}\ . \tag{15}$$

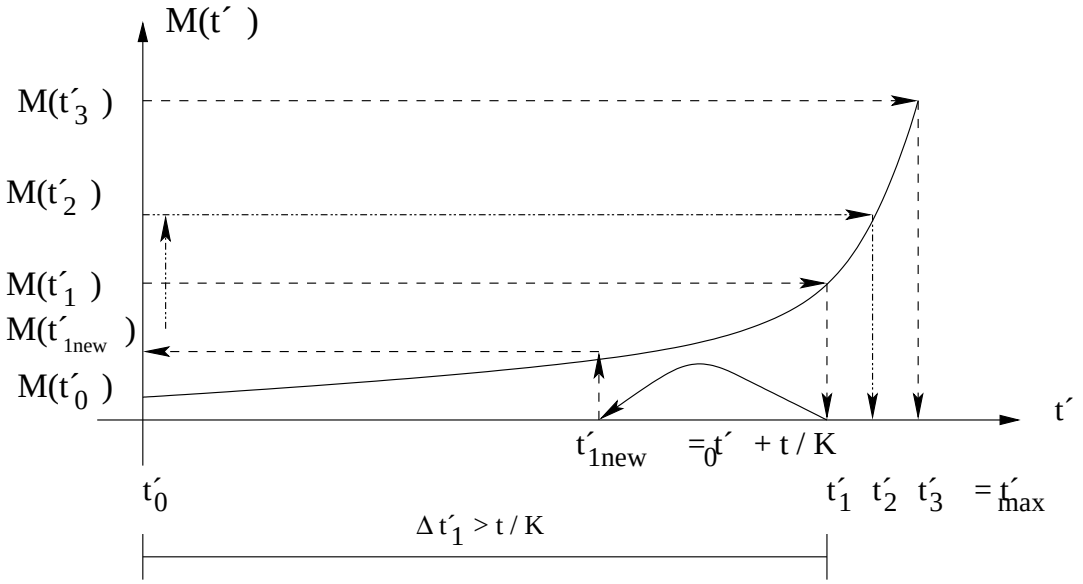

Figure 1: Discretization of the interval $[t'_0,\ t'_{max}]$.

For negative values of t' we adopt de deformation history at $t' = 0$. The first integral in (14) is solved exactly while the second integral is written as

$$\int_0^t \frac{a_1}{We} e^{-\frac{(t-t')}{We}} F(\mathbf{B}_{t'}(t))dt' = \sum_{i=1}^{N} \int_{t'_{i-1}}^{t'_i} \frac{a_1}{We} e^{-\frac{(t-t')}{We}} F(\mathbf{B}_{t'}(t))dt \ . \tag{16}$$

The integrals in (16) can be calculated by a second order integration formula using the undetermined coefficients method or the Trapezoidal Rule. In order to calculate the integrals in (16) the Finger tensor $\mathbf{B}_{t'_i}(t)$ is required. In this work we use the ideas of the deformation fields approach introduced by Peters et al.[9] and improved by Hulsen et al.[14] However, we introduce a modification on the procedure adopted by these authors. We compute the Finger tensor at the past time, t'_i, which is then convected to the time t_{n+1} according to the equation (see Peters et al.[9])

$$\frac{\partial \mathbf{B}_{t'}}{\partial t} + \nabla \cdot (\mathbf{v}\mathbf{B}_{t'}) = (\nabla \mathbf{v})^T \cdot \mathbf{B}_{t'} + \mathbf{B}_{t'} \cdot \nabla \mathbf{v} \ , \tag{17}$$

together with the condition $\mathbf{B}|_{t'=t} = \mathbf{I}$, where $\mathbf{I}$ is the unit tensor. The components of the Finger tensor are calculated and stored for each past time $t'_i, i = 0, 1, \cdots, N$. The corresponding finite difference equations for the calculation of $\mathbf{B}_{t'}(t)$ are given in Section 6.

4 Calculation of the Finger tensor on mesh boundaries

When calculating the Finger tensor using equation (17) we employ a high order upwind method to approximate the convective terms. In this work we use the CUBISTA method (Convergent and Universally Bounded Interpolation Scheme for the Treatment of Advection) developed by Alves et al.[16] This scheme requires the values of the variables either remote-downstream or remote-upstream to the flow. Therefore,

for points near the boundaries the values of the components of the Finger tensor on mesh boundaries are required. These are obtained as follows.

Rigid boundary parallel to the x-axis

On these boundaries we have $u = v = 0 \Longrightarrow \dfrac{\partial u}{\partial x} = \dfrac{\partial v}{\partial x} = \dfrac{\partial v}{\partial y} = 0$ (by continuity). In this case, equation (17) leads to the following equations

$$\frac{\partial}{\partial t} B^{xx}_{t'} = 2\frac{\partial u}{\partial y} B^{xy}_{t'} \,, \qquad \frac{\partial}{\partial t} B^{xy}_{t'} = \frac{\partial u}{\partial y} B^{yy}_{t'} \,, \qquad \frac{\partial}{\partial t} B^{yy}_{t'} = 0 \,. \tag{18}$$

Equations (18) are easily solved using finite differences. The calculation of the Finger tensor on rigid boundaries parallel to the y-axis is similar.

Calculation of the Finger tensor on inflows

On inflows we consider fully developed shear flows. For instance, if we consider inflows parallel to the y-axis, then the Finger tensor is given by (e.g. see Bird et al.[17])

$$B^{xx} = \left(\frac{\partial u}{\partial y}\right)^2 (t - t')^2 + 1 \,; \quad B^{xy} = \left(\frac{\partial u}{\partial y}\right)(t - t') \,; \quad B^{yy} = 1 \,. \tag{19}$$

Calculation of the Finger tensor on outflows

On outflows we assume that a homogeneous Neumann condition for the Finger tensor holds. For instance, if the outflow is parallel to the y-axis, we have

$$\frac{\partial B^{xx}}{\partial y} = \frac{\partial B^{xy}}{\partial y} = \frac{\partial B^{yy}}{\partial y} = 0 \,. \tag{20}$$

5 Numerical method

In order to solve equations (8)-(11) we use the ideas presented by Tomé et al.[7] We solve the momentum equations together with the mass conservation equation followed by the solution of the equations related to the K-BKZ model, as follows.

Given the velocity field and the extra-stress tensor at time t_n, with the respective boundary conditions we use the following procedure to compute the velocity field, pressure and extra stress tensor at the time $t_{n+1} = t_n + \Delta t$.

Step 1 Let $\widetilde{p}$ be a pressure field that satisfies the correct pressure condition on the free surface. This pressure field is computed from the free surface stress condition $\mathbf{n} \cdot (\boldsymbol{\sigma} \cdot \mathbf{n}) = 0$.

Step 2 Calculate the intermediate velocity field, $\tilde{\mathbf{v}}(\mathbf{x}, t_{n+1})$, using equations

$$\frac{\partial \tilde{u}}{\partial t} = -\frac{\partial \widetilde{p}}{\partial x} - \frac{\partial (u^2)}{\partial x} - \frac{\partial (uv)}{\partial y} + \frac{1}{Re}\left(\frac{\partial^2 u}{\partial x^2} + \frac{\partial^2 u}{\partial y^2}\right) + \frac{\partial S^{xx}}{\partial x} + \frac{\partial S^{xy}}{\partial y} + \frac{1}{Fr^2} g_x \tag{21}$$

$$\frac{\partial \tilde{v}}{\partial t} = -\frac{\partial \widetilde{p}}{\partial y} - \frac{\partial (uv)}{\partial x} - \frac{\partial (v^2)}{\partial y} + \frac{1}{Re}\left(\frac{\partial^2 v}{\partial x^2} + \frac{\partial^2 v}{\partial y^2}\right) + \frac{\partial S^{xy}}{\partial x} + \frac{\partial S^{yy}}{\partial y} + \frac{1}{Fr^2} g_y \tag{22}$$

Step 3 Solve the Poisson equation:

$$\nabla^2\psi(\mathbf{x}, t_{n+1}) = \nabla \cdot \tilde{\mathbf{v}}(\mathbf{x}, t_{n+1}) \tag{23}$$

with the condition $\frac{\partial\psi}{\partial n} = 0$ on rigid boundaries and inflows; $\psi = 0$ on the free surface and outflows.

Step 4 Compute the velocity field

$$\mathbf{v}(\mathbf{x}, t_{n+1}) = \tilde{\mathbf{v}}(\mathbf{x}, t_{n+1}) - \nabla\psi(\mathbf{x}, t_{n+1}) \tag{24}$$

Step 5 Compute the pressure

$$p(\mathbf{x}, t_{n+1}) = \widetilde{p}(\mathbf{x}, t_{n+1}) + \frac{\psi(\mathbf{x}, t_{n+1})}{\Delta t} \tag{25}$$

Step 6 Compute the stress-tensor $\boldsymbol{\tau}$ by the following steps:

6.1 Calculate the integration nodes $t'_i,\ i = 1, \cdots, N$, using the procedure described in Section 3

6.2 Compute the components of the Finger tensor on rigid boundaries, inflows and outflows according to the equations presented in Section 4.

6.3 Calculate the components of the Finger tensor $\mathbf{B}_{t'}(t)$ from equation (17).

6.4 Compute the components of extra-stress tensor $\boldsymbol{\tau}(t)$ from (14).

Step 7 Compute the components of the tensor $\mathbf{S}$ by using (11)

Step 8 Update the markers positions: The last step in the calculation is to move the markers to their new positions. This is performed by solving

$$\frac{dx}{dt} = u\ , \qquad\qquad \frac{dy}{dt} = v\ , \tag{26}$$

for each particle. The fluid surface is defined by an ordered list containing these markers and the visualization of the free surface is obtained simply by connecting them by straight lines.

6 Basic finite difference equations

For solving the equations of the numerical method presented in Section 5 we employ the finite difference method on a staggered grid with cell spacing δx and δy. Figure 2a displays the position of the variables in a given cell. We shall be concerned with problems having a moving free surface so that a scheme for identifying the fluid region and the free surface is required. To affect this, the cells within the mesh can be of several types: empty cells (E-cell), full cells (F-cell), surface cells (S-cell), boundary cells (B), inflow cells (I-cell) and outflow cells (O-cells). E-cells do not have fluid while a F-cell contains fluid. S-cells contain fluid and is required to be in contact with an E-cell: these cells contain the fluid free surface. B-cells describe a rigid boundary; I-cell and O-cell are cells simulating inflow and outflow boundaries, respectively. Figure 2b displays the types of cells within the mesh in a given time.

The equations of **Step 1** to **Step 5** and **Step 8** are the same as those used for computing the flow of an Oldroyd-B fluid and the corresponding finite difference equations have been presented by Tomé et al.[7] Therefore, in this work we shall present only the finite difference equations for calculating **Step 6** and **Step 7**, as follows:

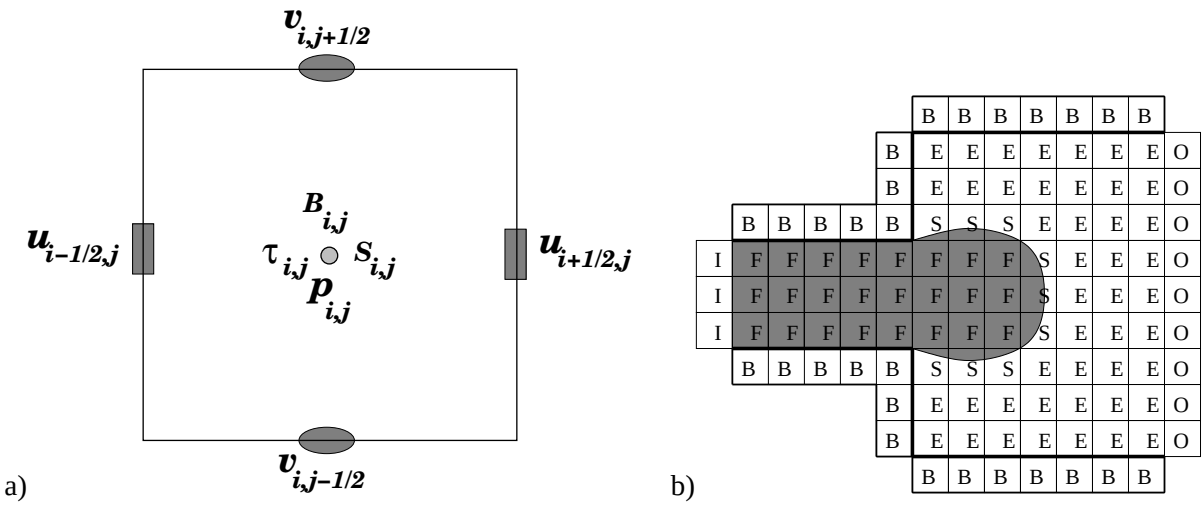

Figure 2: a) Typical cell for fluid flow calculation. b) Types of cells within the mesh.

Approximation of the Finger tensor

The Finger tensor (see equation (17)) is approximated as follows: the time derivative is calculated using the explicit Euler method while the derivatives $\frac{\partial u}{\partial x}$, $\frac{\partial v}{\partial y}$, $\frac{\partial u}{\partial y}$ and $\frac{\partial v}{\partial x}$ are computed using central differences. For the convective terms of equation (17) we employ the high order upwind scheme CUBISTA (see Alves et al.[16]). Details of the implementation of the CUBISTA scheme for two-dimensional flows can be found in.[18] Therefore, the components of the Finger tensor are calculated by

$$\begin{aligned} B^{xx}_{t'_k}(t_{n+1}) = \; & B^{xx}_{t'_k}(t_n) + \Delta t \left\{ -\texttt{conv}(uB^{xx}_{t'_k}(t_n)) - \texttt{conv}(vB^{xx}_{t'_k}(t_n)) \right. \\ & \left. +2\left[\frac{\partial u}{\partial x}|_{i,j} B^{xx}_{t'_k}(t_n)|_{i,j} + \frac{\partial u}{\partial y}|_{i,j} B^{xy}_{t'_k}(t_n)|_{i,j} \right] \right\} \end{aligned} \tag{27}$$

$$\begin{aligned} B^{xy}_{t'_k}(t_{n+1}) = \; & B^{xy}_{t'_k}(t_n) + \Delta t \left\{ -\texttt{conv}(uB^{xy}_{t'_k}(t_n)) - \texttt{conv}(vB^{xy}_{t'_k}(t_n)) \right. \\ & \left. +\frac{\partial v}{\partial x}|_{i,j} B^{xx}_{t'_k}(t_n)|_{i,j} + \frac{\partial u}{\partial y}|_{i,j} B^{yy}_{t'_k}(t_n)|_{i,j} \right\} , \end{aligned} \tag{28}$$

$$\begin{aligned} B^{yy}_{t'_k}(t_{n+1}) = \; & B^{yy}_{t'_k}(t_n) + \Delta t \left\{ -\texttt{conv}(uB^{yy}_{t_{n-s_k}}) - \texttt{conv}(vB^{yy}_{t_{n-s_k}}) \right. \\ & \left. +2\left[\frac{\partial v}{\partial x}|_{i,j} B^{xy}_{t'_k}(t_n)|_{i,j} + \frac{\partial v}{\partial y}|_{i,j} B^{yy}_{t'_k}(t_n)|_{i,j} \right] \right\} , \end{aligned} \tag{29}$$

where

$$\begin{aligned} \texttt{conv}(uB^{xx}_{t'_k}(t_n)) &= \frac{\partial}{\partial x}(uB^{xx}_{t'_k}(t_n)),\ \texttt{conv}(vB^{xx}_{t'_k}(t_n)) = \frac{\partial}{\partial y}(vB^{xx}_{t'_k}(t_n)), \\ \texttt{conv}(uB^{xy}_{t'_k}(t_n)) &= \frac{\partial}{\partial x}(uB^{xy}_{t'_k}(t_n)),\ \texttt{conv}(vB^{xy}_{t'_k}(t_n)) = \frac{\partial}{\partial y}(vB^{xy}_{t'_k}(t_n)), \\ \texttt{conv}(uB^{yy}_{t'_k}(t_n)) &= \frac{\partial}{\partial x}(uB^{yy}_{t'_k}(t_n)),\ \texttt{conv}(vB^{yy}_{t'_k}(t_n)) = \frac{\partial}{\partial y}(vB^{yy}_{t'_k}(t_n)) , \end{aligned}$$

$$\frac{\partial u}{\partial x}|_{i,j} = \frac{\left(u_{i+1/2,j} - u_{i-1/2,j}\right)}{\Delta x}\,, \qquad \frac{\partial v}{\partial y}|_{i,j} = \frac{\left(v_{i,j+1/2} - v_{i,j-1/2}\right)}{\Delta y},$$
$$\frac{\partial u}{\partial y}|_{i,j} = \frac{\left(u_{i,j+1/2} - u_{i,j-1/2}\right)}{\Delta y}\,, \qquad \frac{\partial v}{\partial x}|_{i,j} = \frac{\left(v_{i+1/2,j} - v_{i-1/2,j}\right)}{\Delta x}\,.$$

Terms which are not defined at cell position are obtained by averaging. For instance,

$$u_{i,j+\frac{1}{2}} = 0.25\left(u_{i+\frac{1}{2},j} + u_{i+\frac{1}{2},j+1} + u_{i-\frac{1}{2},j} + u_{i-\frac{1}{2},j+1}\right)\,,$$
$$v_{i+\frac{1}{2},j} = 0.25\left(v_{i,j+\frac{1}{2}} + u_{i+1,j+\frac{1}{2}} + v_{i,j-\frac{1}{2}} + u_{i+1,j-\frac{1}{2}}\right)\,.$$

These equations are solved for each past time $t'_k, k = 0, 1, \cdots, N$. They convect the fields $\mathbf{B}_{t'_k}(t_n)$ at past times t'_k to the next time $t = t_{n+1}$. Having calculated $\mathbf{B}_{t'_k}(t_{n+1})$, the new values of $t'_k(t_{n+1})$ in the interval $[0,\ t_{n+1}]$ are obtained using the procedure described in Section 3 and the values of $\mathbf{B}_{t'_k(t_{n+1})}(t_{n+1})$ are then computed using linear interpolation. For instance, if we consider simple shear flows, figure 3 shows how we compute the component B^{xy} at the times $t'_k(t_{n+1})$. Having computed the Finger tensor for $t'_k(t_{n+1}), k = 0, 1, \cdots, N$, the values of the stress tensor are obtained by solving equation (14) componentwise according to equation (10) (see Section 3).

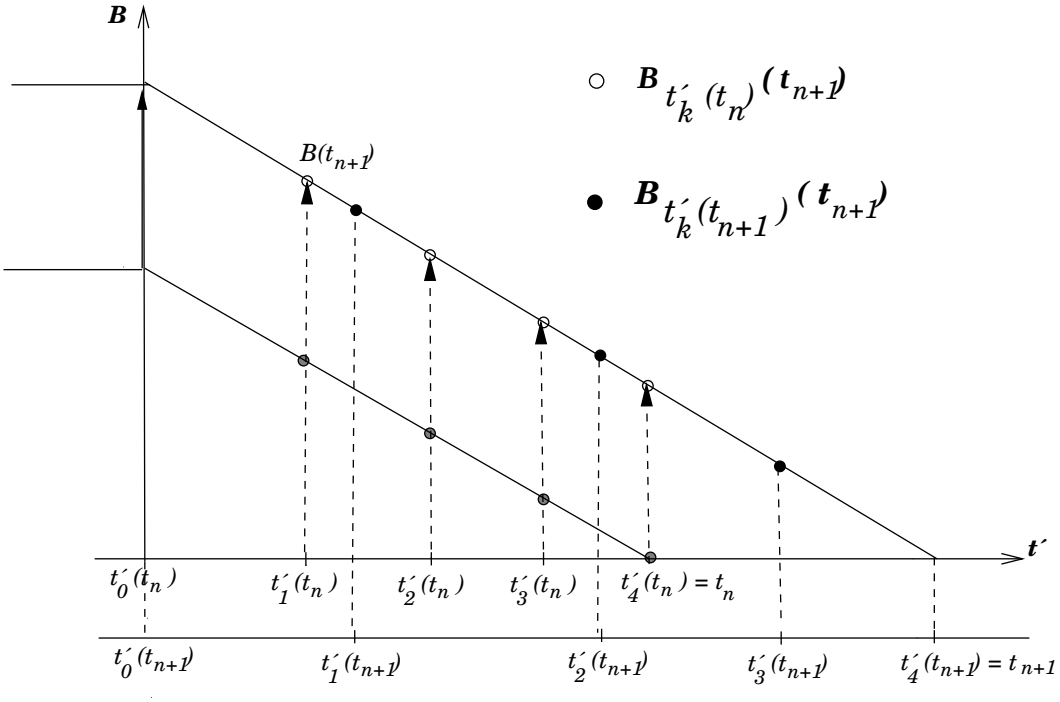

Figure 3: Calculation of the Finger tensor at times $t'_k(t_{n+1})$ by using linear interpolation. For times $t' < t'_0$ we used the deformation at the time t'_0.

Approximation of the free surface stress conditions

By using two-dimensional cartesian coordinates, the stress conditions (12) can be written as

$$-\widetilde{p}+\frac{2}{Re}\left[\frac{\partial u}{\partial x}n_x^2+\left(\frac{\partial u}{\partial y}+\frac{\partial v}{\partial x}\right)n_xn_y+\frac{\partial v}{\partial y}n_y^2\right]+S^{xx}n_x^2+2\,S^{xy}n_xn_y+S^{yy}n_y^2=0, \tag{30}$$

$$\frac{1}{Re}\left[2\left(\frac{\partial u}{\partial x}-\frac{\partial v}{\partial y}\right)n_xn_y+\left(\frac{\partial u}{\partial y}+\frac{\partial v}{\partial x}\right)(n_y^2-n_x^2)\right]+(S^{xx}-S^{yy})n_xn_y+S^{xy}(n_y^2-n_x^2)=0. \tag{31}$$

To apply these conditions we follow the ideas of Tomé et al.[7] We assume the mesh is sufficiently fine so that, locally, the free surface can be approximated by vertical/horizontal and 45^0-sloped surfaces. For these surfaces, the normal vector takes the form of $\mathbf{n}=(0,\ 1)$ or $\mathbf{n}=(1,\ 0)$ or $\mathbf{n}=(\pm\frac{\sqrt{2}}{2},\ \pm\frac{\sqrt{2}}{2})$. These surfaces are identified by S-cells having only one face in contact with an E-cell or S-cells having two-adjacent faces in contact with E-cell faces (see figure 4). For instance, if consider the S-cell having the $(j+\frac{1}{2})$-face in contact with an E-cell in figure 4a then we take $\mathbf{n}=(0,\ 1)$ and equations (30)-(31) reduce to

$$-\widetilde{p}+\frac{2}{Re}\frac{\partial v}{\partial y}+S^{yy}=0\,, \tag{32}$$

$$\frac{1}{Re}\left(\frac{\partial u}{\partial y}+\frac{\partial v}{\partial x}\right)+S^{xy}=0\,. \tag{33}$$

Considering figure 4a, the values of $v_{i,j+\frac{1}{2}}$, $u_{i+\frac{1}{2},j+1}$ and $\widetilde{p}_{i,j}$ are required. They are calculated as follows: the value of $v_{i,j+\frac{1}{2}}$ is obtained by applying the continuity equation at the cell centre while $u_{i+\frac{1}{2},j+1}$ is computed by discretizing equation (33) at the cell corner $(i+\frac{1}{2},j+\frac{1}{2})$ yielding

$$\begin{aligned} v_{i,j+\frac{1}{2}} &= v_{i,j-\frac{1}{2}}-\frac{\delta y}{\delta x}(u_{i+\frac{1}{2},j}-u_{i-\frac{1}{2},j})\,,\\ u_{i+\frac{1}{2},j+1} &= u_{i+\frac{1}{2},j}-\frac{\delta y}{\delta x}(v_{i+1,j+\frac{1}{2}}-v_{i,j+\frac{1}{2}})-\delta y\,Re\,S^{xy}_{i+\frac{1}{2},j+\frac{1}{2}}\,, \end{aligned} \tag{34}$$

respectively. The pressure $\widetilde{p}_{i,j}$ is then calculated from (32) applied at the cell centre, giving

$$\widetilde{p}_{i,j}=\frac{2}{Re}\frac{(v_{i+1,j\frac{1}{2}}-v_{i,j+\frac{1}{2}})}{\delta y}+S^{yy}_{i,j}\,. \tag{35}$$

Other types of S-cells having only one face in contact with an E-cell face is treated similarly. For S-cells with two adjacent faces in contact with E-cell faces the treatment is similar. For instance, for the S-cell shown in figure 4b we take $\mathbf{n}=(\frac{\sqrt{2}}{2},\ \frac{\sqrt{2}}{2})$ and the stress conditions (30)-(31) become

$$-\widetilde{p}+\frac{1}{Re}\left(\frac{\partial u}{\partial y}+\frac{\partial v}{\partial x}\right)+\frac{1}{2}(S^{xx}+2S^{xy}+S^{yy})=0\,, \tag{36}$$

$$\frac{1}{Re}\left(\frac{\partial u}{\partial x}+\frac{\partial v}{\partial y}\right)+\frac{1}{2}(S^{xx}-S^{yy})=0\,. \tag{37}$$

The values of $u_{i+\frac{1}{2},j}$ and $v_{i,j+\frac{1}{2}}$ are obtained by applying the mass conservation equation and stress condition (37) at the cell centre, giving

$$\frac{(u_{i+\frac{1}{2},j} - u_{i-\frac{1}{2},j})}{\delta x} + \frac{(v_{i,j+\frac{1}{2}} - v_{i,j-\frac{1}{2}})}{\delta y} = 0\,, \tag{38}$$

$$\frac{(u_{i+\frac{1}{2},j} - u_{i-\frac{1}{2},j})}{\delta x} - \frac{(v_{i,j+\frac{1}{2}} - v_{i,j-\frac{1}{2}})}{\delta y} = \frac{Re}{2}(S^{xx}_{i,j} - S^{yy}_{i,j})\,. \tag{39}$$

Equations (38) and (39) form a (2×2)-linear system for the unknowns $u_{i+\frac{1}{2},j}$ and $v_{i,j+\frac{1}{2}}$ yielding

$$u_{i+\frac{1}{2},j} = u_{i-\frac{1}{2},j} + \frac{\delta x}{4}\,Re\,(S^{xx}_{i,j} - S^{yy}_{i,j})\,, \qquad v_{i,j+\frac{1}{2}} = v_{i,j-\frac{1}{2}} - \frac{\delta y}{\delta x}(u_{i+\frac{1}{2},j} - u_{i-\frac{1}{2},j})\,. \tag{40}$$

After calculating $u_{i+\frac{1}{2},j}$ and $v_{i,j+\frac{1}{2}}$, the pressure at the cell centre is computed from (36) applied at the cell centre which gives

$$\widetilde{p}_{i,j} = \frac{1}{Re}\left[\frac{(u_{i,j} - u_{i,j-1})}{\delta y} + \frac{(v_{i,j} - v_{i-1,j})}{\delta x}\right] + \frac{1}{2}(S^{xx}_{i,j} + 2S^{xy}_{i,j} + S^{yy}_{i,j}) \tag{41}$$

where the values of $u_{i,j}$ and $v_{i,j}$ are given by

$$u_{i,j} = \frac{u_{i+\frac{1}{2},j} + u_{i-\frac{1}{2},j}}{2}\,, \qquad v_{i,j} = \frac{v_{i,j+\frac{1}{2}} + v_{i,j-\frac{1}{2}}}{2}\,.$$

Other types of S-cells having two adjacent faces in contact with E-cell faces are treated similarly. For surface cells having two-opposite faces in contact with E-cells faces we do not have an approximation for the normal vector. In these cells, the pressure $\widetilde{p}_{i,j}$ is set to zero and one velocity is adjusted so that the continuity equation is satisfied for these cells.

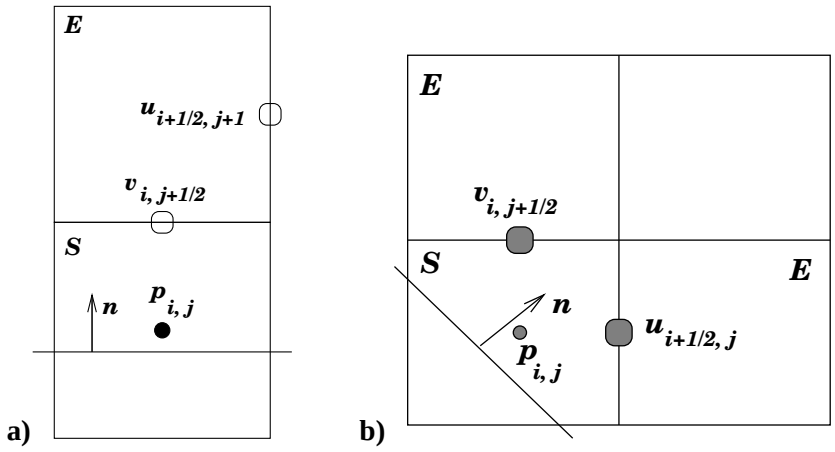

Figure 4: S-cells having one and two faces in contact with E-cell faces.

7 Numerical results

In this section we present numerical results for fully developed channel flow and for the planar 4:1 contraction problem. We also present numerical results showing the simulation of jet buckling using the K-BKZ constitutive equation. The results on the channel flow are performed to study the convergence of the numerical method presented in this paper while the simulation of the flow through a planar 4:1 contraction shows the effect of the Weissenberg number on the size of the corner vortex.

In the results that follow we used $U = 1\,ms^{-1}$, $L = 0.01\,m$, $\rho_0 = 1,000kg/m^3$ and $\eta_0 = 10Pa.s$ so that $Re = \frac{\rho_0\,U\,L}{\eta_0} = 1$.

Fully developed channel flow

We applied the numerical technique presented in this paper to simulate the flow in a two-dimensional channel governed by the K-BKZ model. We considered a 2D-channel formed by two parallel walls at a distance L from each other and having a length of $10\,L$. In the K-BKZ equation we used $\alpha = 500$, $\beta = 0.1$, $a_1 = 2,000$ and $\lambda_1 = 0.005$ so that the Weissenberg number was $We = \lambda_1 \frac{U}{L} = 0.5$.

We solved this problem using three different meshes: **Mesh M1** with 10×100 cells; **Mesh M2** with 20×200 cells and **Mesh M3** with 30×300 cells. The simulation started with the channel full with null velocity. The Finger tensor was set to unit in all the cells and a Newtonian parabolic profile for the velocity was imposed on the inflow. We ran this problem until the contour lines were parallel indicating that the steady state was reached. Under these conditions, we expect that the numerical solution converged to the respective exact solution of the K-BKZ model for the flow within the channel. Indeed, figure 5 shows the values of the components of the extra-stress tensor and the component u of the velocity obtained in the middle of the channel using the three meshes. As we can see in figure 5, the agreement between the three solutions is very good which shows that the numerical method developed in this work converges as the mesh is refined.

Simulation of the flow through a planar 4:1 contraction

We considered the flow through a planar 4:1 contraction. A schematic diagram of this geometry is displayed in figure 6. At fluid entrance we imposed a parabolic Poiseuille flow and on the contraction walls the velocity field satisfies the no-slip condition. To simulate this problem we used a mesh with 320×80 cells and the Reynolds number was fixed to $Re = 1$ as in the channel flow simulation ($U = 1.0, L = 0.01, \eta_0 = 10.0, \rho_0 = 1,000$). We solved this problem using three Weissenberg numbers: $We = 0.01$ so that we used $a_1 = 10^5$ and $\lambda_1 = 10^{-4}$, $We = 1.0$ ($a_1 = 1,000$ and $\lambda_1 = 10^{-4}$) and $We = 2$ ($a_1 = 500$ and $\lambda_1 = 0.02$). The parameters α and β were set to 500 and 0.1, respectively. We ran this problem until the steady state was reached. The results are displayed in figure 7 (due to symmetry, only the superior half of the flow domain is shown). We can observe in figure 7 that the size of the corner vortex decreases as We increases. These results agree with those published in the literature (eg. see Phillips and Williams[19]).

Numerical simulation of jet buckling

The phenomenon of jet buckling appears in various industrial applications and consequently it has been the subject of several investigators.[20–22] However, although this problem has not been fully understood Cruickshank and Munson[20] and Cruickshank[23] have presented experimental and theoretical

estimates for predicting the buckling of Newtonian jets. In particular, they found that a two-dimensional Newtonian jet will undergo buckling if the following conditions are satisfied:

$$Re < 0.56 \text{ and } H/L > 3\,\pi \tag{42}$$

where H is the height of the inlet and L is the inlet size.

To illustrate the effect of buckling on thin jets governed by the K-BKZ constitutive equation, we performed two simulations which showed different behaviour from each other. We considered an empty box of dimensions of 5 cm $\times$ 10 cm with an inlet situated at the box entrance. The size of the inlet was $L = 5$ mm and the velocity at the inlet was $U = 1$ ms^{-1}. In the first simulation we employed a Newtonian jet while in the second simulation the fluid was modeled by the K-BKZ equation. In these simulations the lengh and velocity scales were L and U, respectively. The Newtonian viscosity and the parameters for the K-BKZ model were defined so that the Reynolds number was $Re = 0.6$ for both simulations and the Weissenberg number was $We = 0.5$. Thus, the Cruickshank's restriction on the Reynolds number is not satisfied and we do not expect that the Newtonian jet will present the buckling phenomenon. However, for the viscoelastic jet governed by the K-BKZ constitutive equation we can not predict the buckling phenomenon since Cruickshank's results are restricted to Newtonian jets. The results of these simulations are displayed in figure 8. As we can see in figure 8 the Newtonian jet did not buckle (confirming Cruickshank's prediction) while the viscoelastic jet governed by the K-BKZ constitutive equation did undergo the buckling phenomenon. We believe the K-BKZ jet buckled due to the high extensional viscosity developed within the jet as it flows onto the rigid plate.

8 Concluding remarks

This paper presented a numerical technique for simulating viscoelastic flows governed by the integral K-BKZ constitutive equation. The numerical method developed is based on the finite difference method on a staggered grid. The equation of motion was solved using the ideas of Tomé et al.[7] and the fluid was modeled by the Marker-and-Cell method using marker particles on the fluid surface only (see Tomé et al.[24]). The flow in a two-dimensional channel was simulated using mesh refinement and the results were good showing the convergence of the numerical method developed in this work. The simulation of the flow through a planar 4:1 contraction was simulated for various values of the Weissenberg number and the results showed that the size of the corner vortex diminishes as the Weissenberg number is increased: this result is in agreement with those published in the literature. Furthermore, we presented the simulation of thin jets impinging onto a rigid plate. It is known that under certain conditions based on the jet diameter and on the Reynolds number the jet will not flow radially and therefore undergo buckling. Indeed, Cruickshank's[23] presented an upper limit for the Reynolds number so that for a Reynolds number beyond this limit a thin Newtonian jet will not produce the phenomenon of jet buckling. Two simulations were performed in which the Reynolds number was above Cruickshank's[23] prediction. The results showed that the Newtonian jet did not buckle confirming Cruickshank's prediction. However, the thin jet modeled by the K-BKZ constitutive equation produced jet buckling. We believe this was due to the high extensional viscosity developed at the time the jet touched the rigid plate.

9 Acknowledgments

The first author would like to thank the financial support of CAPES. The authors also thank the support of the Brazilian funding agencies CNPq (research grants No. 474040/2003-8, 523141/94) and FAPESP (research grant No. 2000/03385-0).

REFERENCES

[1] J.M. Marchal and M.J. Crochet. A new mixed finite element for calculating viscoelastic flow. *J. Non-Newtonian Fluid Mechanics*, **26**, 77–114 (1987).

[2] V. Ngamaramvaranggul and M.F. Webster. Computation of free surface flows with a taylor-galerkin/pressure correction algorithm. *Intern. J. Numer. Meth. Fluids*, **33**, 993–1026 (2000).

[3] V. Ngamaramvaranggul and M.F. Webster. Simulation of coating flows with slip effects. *Intern. J. Numer. Meth. Fluids*, **33**, 961–992 (2000).

[4] B. Caswell and M. Viriyayuthakon. Finite element simulation of die swell for a maxwell fluid. *J. Non-Newtonian Fluid Mechanics*, **12**, 13–29 (1983).

[5] G. Mompean and M. Deville. Unsteady finite volume of oldroyd-b fluid through a three-dimensional planar contraction. *J. Non-Newtonian Fluid Mechanics*, **72**, 253–279 (1997).

[6] S.-C. Xue, N. Phan-Thien, and R.I. Tanner. Numerical study of secondary flows of viscoelastic fluid in straight pipes by an implicit finite volume method. *J. Non-Newtonian Fluid Mechanics*, **59**, 191–213 (1995).

[7] M.F. Tomé, N. Mangiavacchi, J.A. Cuminato, A. Castelo, , and S. McKee. A finite difference technique for simulating unsteady viscoeslastic free surface flows. *J. Non-Newtonian Fluid Mechanics*, **106**, 61–96 (2002).

[8] M. Normandin, J.-R. Clermont, J. Guillet, and C. Raveyre. Three-dimensional extrudate swell experimental and numerical study of a polyethylene melt obeying a memory-integral equation. *J. Non-Newtonian Fluid Mechanics*, **87**, 1–25 (1999).

[9] E.A.J.F. Peters, M.A. Hulsen, and B.H.A.A. van den Brule. Instationary Eulerian viscoelastic flow simulation using time separable Rivlin-Sawyers constitutive equations. *J. Non-Newtonian Fluid Mechanics*, **89**, 209–228 (2000).

[10] X.-L. Luo. A control volume approach for integral viscoelastic models and its application to contraction flow of polymer melts. *J. Non-Newtonian Fluid Mechanics*, **64**, 173–189 (1996).

[11] P. Olley and P.D. Coates. An approximation to the kbkz constitutive equation. *J. Non-Newtonian Fluid Mechanics*, **69**, 239–254 (1997).

[12] E. Mitsoulis. Numerical simulation of entry flow of fluid s1. *J. Non-Newtonian Fluid Mechanics*, **78**, 187–201 (1998).

[13] hell and heel1. teste non-newt. *J. Non-Newtonian Fluid Mechanics*, **1**, 1–10 (1999).

[14] M.A.Hulsen, E.A.J.F. Peters, and B.H.A.A. van den Brule. A new approach to the deformation fields method for solving complex flows using integral constitutive equations. *J. Non-Newtonian Fluid Mechanics*, **98**, 201–221 (2001).

[15] A. C. Papanastasiou, L. Scriven, and C. Makosco. An integral constitutive equation for mixed flows: Viscoelastic characterization. *Journal of Rheology*, **27**, 387–410 (1983).

[16] M.A. Alves, P.J. Oliveira, and F.T. Pinho. A convergent and universally bounded interpolation scheme for treatment of advection. *Int. J. Numer. Meth. Fluids*, **41**, 47–75 (2003).

[17] R. B. Bird, R. C. Armstrong, and O. Hassager. *Dynamics of Polymeric Liquids*. John Wiley &

Sons, (1987).

[18] A. C. Brandi. Estratégias upwind e modelagem $k - \epsilon$ para simulação numérica de escoamentos com superfícies livres em altos números de reynolds. Master's thesis, Departamento de Ciências de Computação e Estatística - ICMC - USP, (2005).

[19] T. N. Phillips and A. J. Williams. Viscoelastic flow through a planar contraction using a semi-lagrangian finite volume method. *J. Non-Newtonian Fluid Mechanics*, **87**, 215–226 (1999).

[20] J.O. Cruickshank and B.R. Munson. Viscous-fluid buckling of plane and axisymmetric jets. *Journal of Fluid Mechanics*, **113**, 221–239 (1981).

[21] M. F. Tomé and S. McKee. Numerical simulation of viscous flow: Buckling of planar jets. *Intern. J. Numer. Meth. Fluids*, **29**, 705–718 (1999).

[22] N. M. Ribe. Periodic folding of viscous sheets. *Physical Review E*, **68**, 0363051–0363056 (1965).

[23] J.O. Cruickshank. Low-reynolds-number instabilities in stagnating jet flows. *Journal of Fluid Mechanics*, **193**, 111–127 (1988).

[24] M.F. Tomé, A. Castelo, J. Murakami, N. Mangiavacchi, J.A. Cuminato, R. Minghim, M.C.F. Oliveira, and S. McKee. Numerical simulation of axisymmetric free surface flows. *J. of Computational Physics*, **157**, 441–472 (2000).

a)

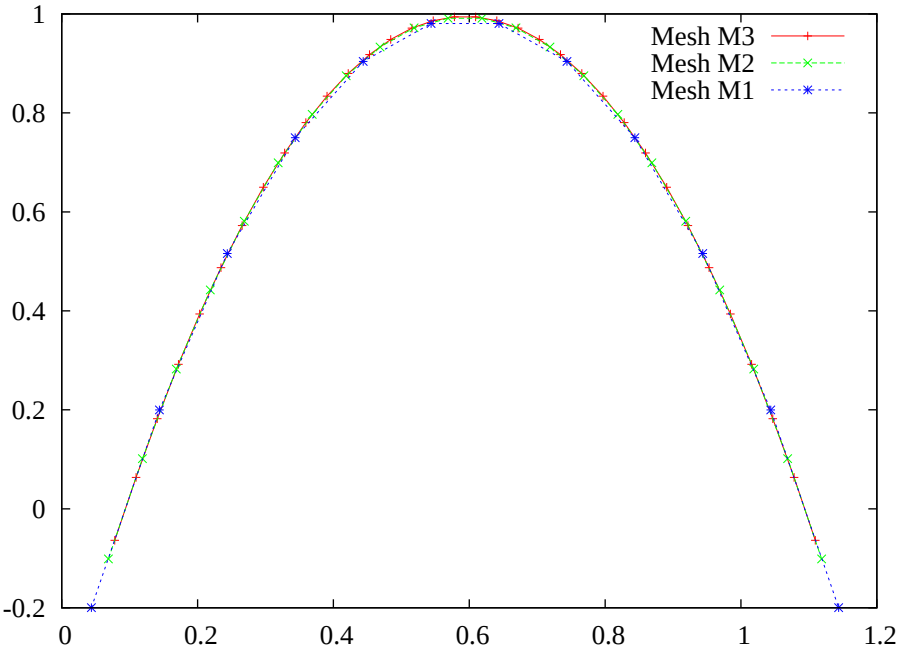

b)

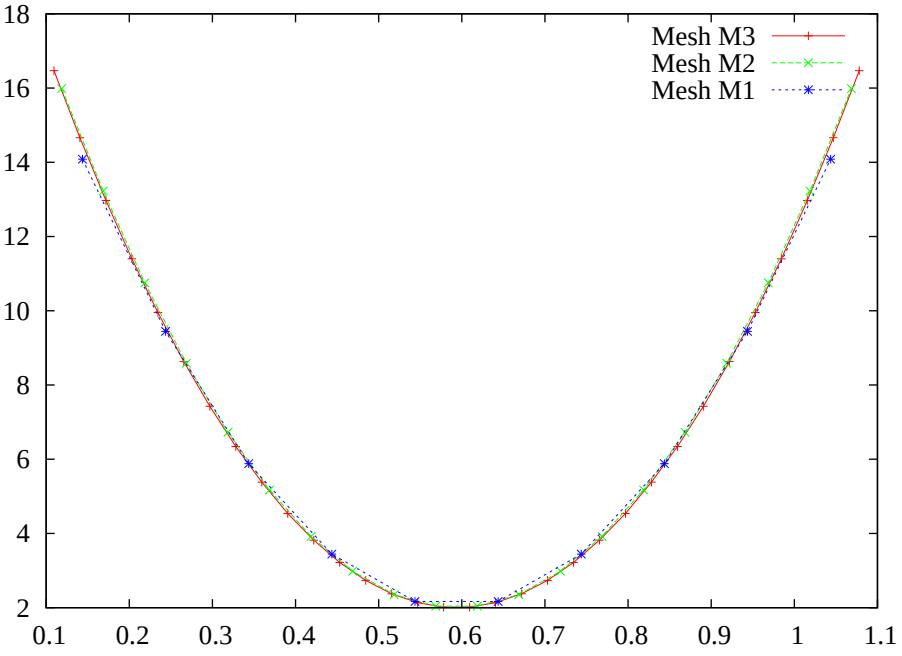

Figure 5: Results for the channel flow simulation. Numerical solution at the middle of the channel using $Re = 1, We = 0.5$ on the three meshes: a)velocity u, b) τ_{xx}, c) τ_{xy}, d) τ_{yy}.

c)

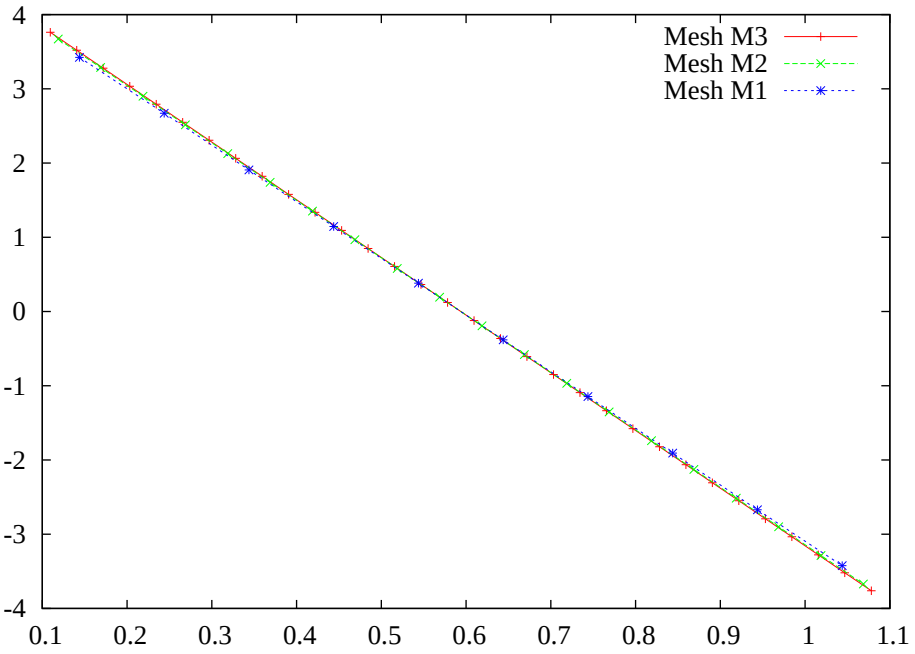

d)

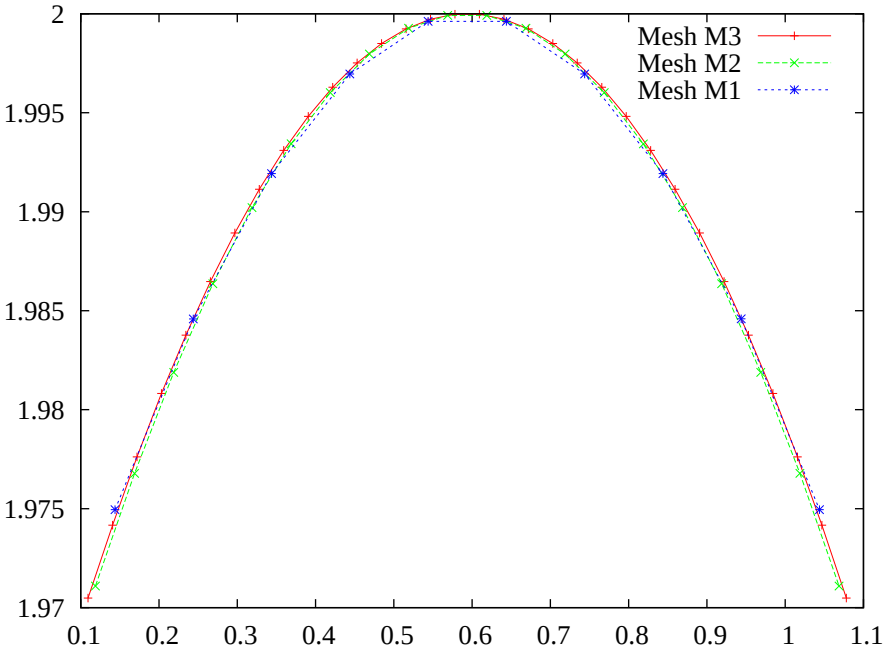

Figure 5: Continued.

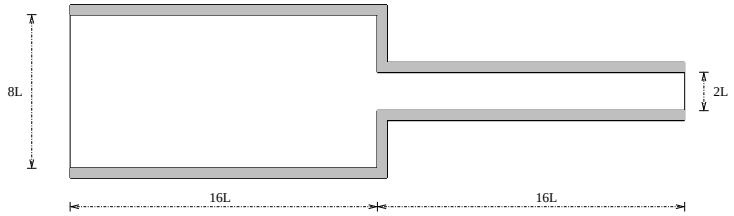

Figure 6: Domain used to simulate the planar 4:1 contraction.

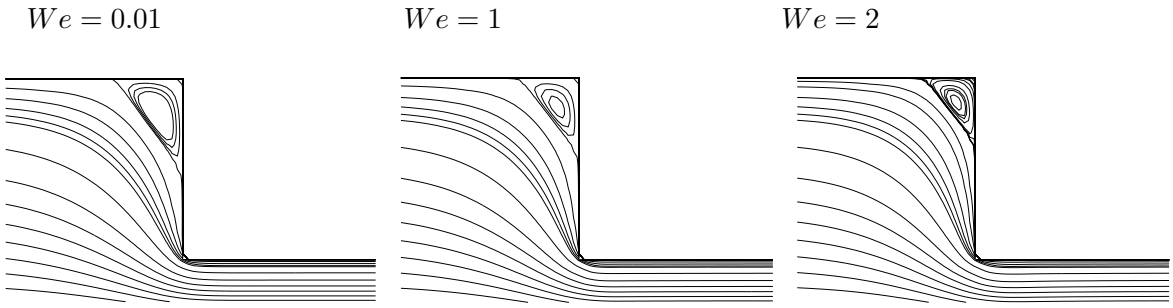

Figure 7: Numerical results for the fbw through a planar 4:1 contraction with $Re = 1$ for increasing values of the Weissenberg number.

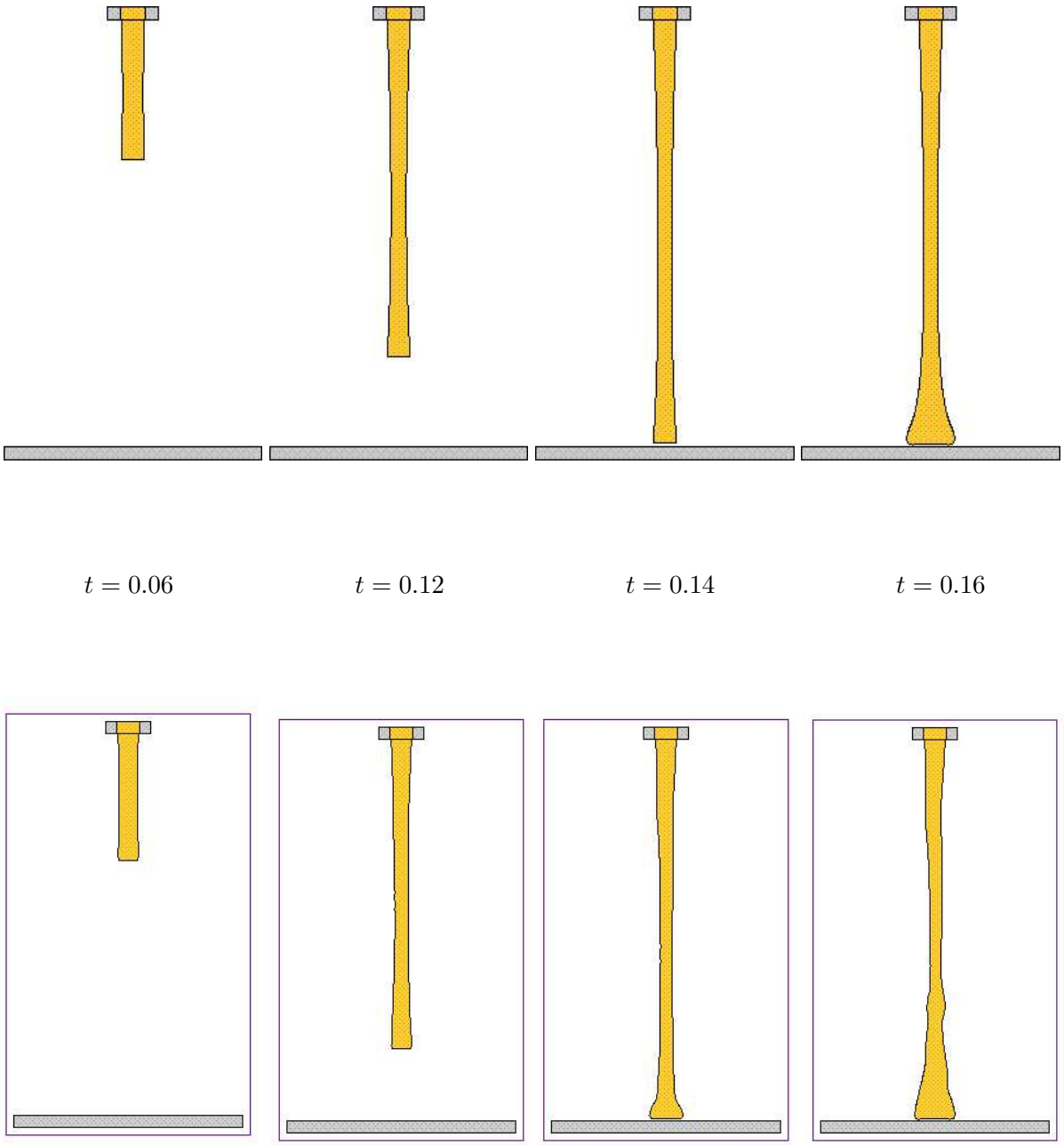

Figure 8: Numerical simulation of jet buckling: Fluid flow visualization at different times. Top row: Newtonian jet with $Re = 0.5$; Bottom row: Viscoelastic jet (K-BKZ model) with $Re = 0.5 and We = 0.5$

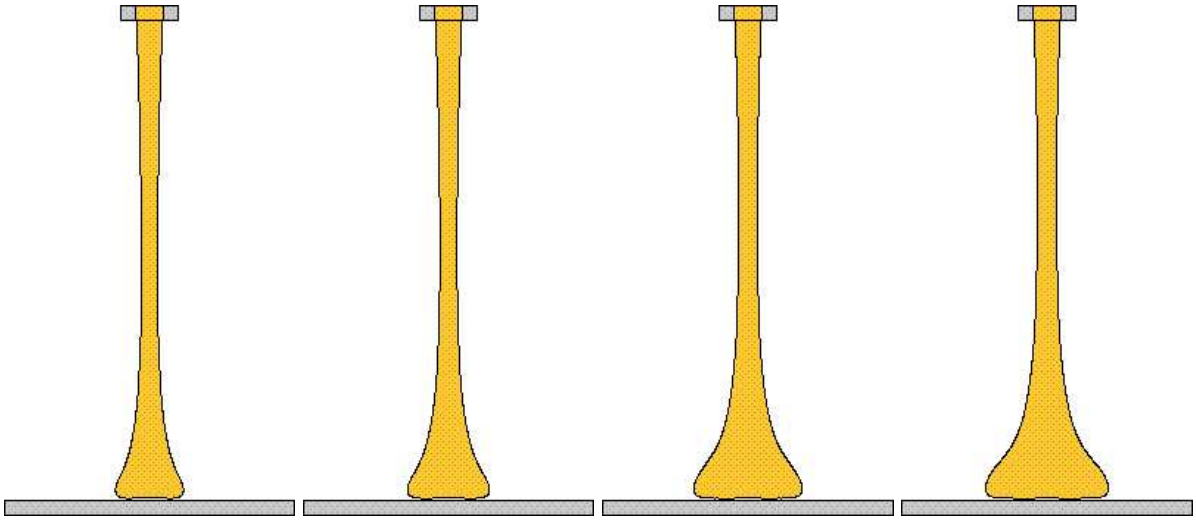

$t = 0.18$ $t = 0.20$ $t = 0.24$ $t = 0.26$

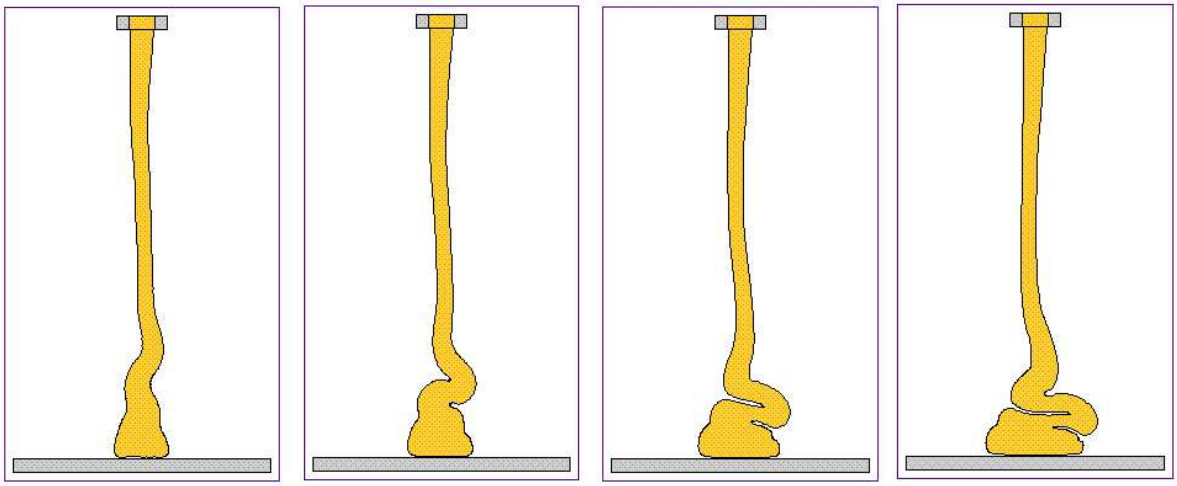

Figure 8: Continued.